THE JOURNAL OF BIOLOGICAL CHEMISTRY VOL. 285, NO. 20, pp. 15201–15208, May 14, 2010

Transcription-dependent Activation of Ataxia Telangiectasia Mutated Prevents DNA-dependent Protein Kinase-mediated Cell Death in Response to Topoisomerase I Poison*[S]

Received for publication, January 6, 2010, and in revised form, March 18, 2010 Published, JBC Papers in Press, March 19, 2010, DOI 10.1074/jbc.M110.101808

Ryo Sakasai[‡1], **Hirobumi Teraoka**[‡], **Masatoshi Takagi**[§], **and Randal S. Tibbetts**[¶]

From the [‡]*Department of Pathological Biochemistry, Medical Research Institute, Tokyo Medical and Dental University, Tokyo 101-0062, Japan, the* [§]*Department of Pediatrics and Developmental Biology, Tokyo Medical and Dental University, Tokyo 113-8519, Japan, and the* [¶]*Department of Pharmacology, University of Wisconsin School of Medicine and Public Health, Madison, Wisconsin 53706*

Camptothecin (CPT) is a topoisomerase I inhibitor, derivatives of which are being used for cancer chemotherapy. CPT-induced DNA double-strand breaks (DSBs) are considered a major cause of its tumoricidal activity, and it has been shown that CPT induces DNA damage signaling through the phosphatidylinositol 3-kinase-related kinases, including ATM (ataxia telangiectasia mutated), ATR (ATM and Rad3-related), and DNA-PK (DNA-dependent protein kinase). In addition, CPT causes DNA strand breaks mediated by transcription, although the downstream signaling events are less well characterized. In this study, we show that CPT-induced activation of ATM requires transcription. Mechanistically, transcription inhibition suppressed CPT-dependent activation of ATM and blocked recruitment of the DNA damage mediator p53-binding protein 1 (53BP1) to DNA damage sites, whereas ATM inhibition abrogated CPT-induced G_1/S and S phase checkpoints. Functional inactivation of ATM resulted in DNA replication-dependent hyperactivation of DNA-PK in CPT-treated cells and dramatic CPT hypersensitivity. On the other hand, simultaneous inhibition of ATM and DNA-PK partially restored CPT resistance, suggesting that activation of DNA-PK is proapoptotic in the absence of ATM. Correspondingly, comet assay and cell cycle synchronization experiments suggested that transcription collapse occurring as the result of CPT treatment are converted to frank double-strand breaks when ATM-deficient cells bypass the G_1/S checkpoint. Thus, ATM suppresses DNA-PK-dependent cell death in response to topoisomerase poisons, a finding with potential clinical implications.

The topoisomerase I (TopI)[2] poison camptothecin (CPT) and its clinically relevant derivatives, topotecan and irinotecan, have been intensively studies for their tumoricidal properties. The molecular target of CPT is TopI, an enzyme that mediates the relaxation of supercoiled DNA (1). This is achieved through the transient introduction of a DNA single-strand break that permits the rotational relaxation of double-stranded DNA. The TopI reaction cycle involves the formation of a transient phosphotyrosyl bond between Tyr^{723} of the enzyme active site and a 3′ DNA end. CPT stabilizes covalent TopI-DNA cleavage complexes (TopI-cc), which are converted into DNA double-strand breaks (DSBs) upon encountering active DNA replication forks (1).

The signaling and repair of CPT-mediated damage have been the focus of intensive research. CPT-induced DSBs possess a single DNA double-strand end (DSE) that is generally not an efficient substrate for nonhomologous end joining DSB repair, which is mediated by DNA-dependent protein kinase (DNA-PK) composed of DNA-PKcs and Ku protein. Instead, CPT-induced DSEs are repaired by homologous recombination (HR) repair, which utilizes a sister chromatid and primes restart of the obstructed DNA replication fork (2, 3). CPT-induced DSEs strongly activate cell cycle checkpoint pathways downstream of the ATM (ataxia telangiectasia mutated) and ATR (ATM and Rad3-related) protein kinases. CPT-induced damage in S phase activates the ATR-Chk1 pathway that mediates S phase arrest (4). Consistent with these important S phase functions, ATR- or Chk1-deficient cells are exquisitely sensitive to TopI poisons (4, 5).

In addition to replication-mediated DNA damage, TopI-cc pose a block to processive RNA polymerase complexes, and the collision of RNA polymerase with TopI-cc results in transcription-mediated DNA damage (6). Although the mechanisms of transcription-coupled damage and signaling are not well understood, recent studies suggest a new role for the ATM protein kinase. CPT-induced activation of ATM is suppressed by inhibitors of transcription, and it has been proposed that ATM responds to RNA·DNA hybrid R-loops that form at stalled RNA polymerase II transcription bubbles (7). However, the detection and signaling of CPT-induced, transcription-dependent DNA damage are not well understood, nor is it clear

* This work was supported, in whole or in part, by National Institutes of Health Grant CA124722. This work was also supported by a grant from the American Cancer Society, a Shaw Scientist Award (to R. S. T.) from the Greater Milwaukee Foundation, and by Grant-in-aid 20659047 from Japan Society for the Promotion of Science for Exploratory Research (to H. T.).

[S] The on-line version of this article (available at http://www.jbc.org) contains supplemental Figs. S1–S5.

[1] To whom correspondence should be addressed: Dept. of Molecular Oncology, Graduate School of Medical Sciences, Kyushu University, Fukuoka 812-8582, Japan. E-mail: sakasai@surg2.med.kyushu-u.ac.jp.

[2] The abbreviations used are: TopI, topoisomerase I; TopI-cc, TopI cleavage complex; CPT, camptothecin; DSB, double-strand break; DSE, double-strand end; DNA-PK, DNA-dependent protein kinase; HR, homologous recombination; ATM, ataxia telangiectasia mutated; ATR, ATM and Rad3-related; DRB, 5,6-dichloro-1-β-D-ribofuranosylbenzimidazole; HU, hydroxyurea; siRNA, small interfering RNA; BrdUrd, bromodeoxyuridine; IR, ionizing radiation; 53BP1, p53-binding protein 1; RPA2, replication protein A2.

whether transcription-mediated DNA damage contributes significantly to CPT cytotoxicity.

In this study, we investigated transcription-dependent and -independent pathways activated by CPT in human cells. We show that ATM is critically important for initiation of the G_1/S phase checkpoint in response to CPT and that transcription-dependent activation of ATM in G_1 phase suppresses DNA strand breakage leading to DNA-PK activation in S phase cells. These findings have implications for understanding CPT tumoricidal activity.

EXPERIMENTAL PROCEDURES

Cell Culture and Irradiation—HeLa, U2OS, and HCT116 cells were obtained from American Type Culture Collection and maintained in Dulbecco's modified Eagle's medium with 10% fetal bovine serum. SV40-transformed GM00637H (ATM+), GM05849C (ATM−), (obtained from Coriell Cell Repositories), and hTERT-immortalized SuSa/Tn (ATM+), AT1OS/Tn (ATM−) (kindly provided by Dr. K Ishizaki) (8) were cultured in Dulbecco's modified Eagle's medium with 10% fetal bovine serum. Cells were UV- and IR-irradiated as reported (9). CPT, VP-16, 5,6-dichloro-1-β-D-ribofuranosylbenzimidazole (DRB), KU-55933, NU7026, hydroxyurea (HU), and thymidine were purchased from Sigma. To knock down TopBP1 and RNF8 expression, siRNA SMART pool targeting each gene (Dharmacon) was used. siRNAs were transfected as described (10).

Antibodies and Immunofluorescence—Antibodies were obtained from following suppliers: Bethyl Laboratories (p53-binding protein 1 (53BP1), A300-272A), Oncogene (replication protein A (RPA), Ab-3; BrdUrd, Ab-2), Millipore (γH2AX, JBW301), Calbiochem (Rad51, PC130), Abcam (phospho-DNA-PKcs, ab18192, Chk2, ab8108), R&D Systems (phospho-ATM, AF-165; phospho-Chk1 Ser^{317}, AF-2054; phospho-Chk2, AF-1626), GeneTex (ATM, GTX70103), Thermo Scientific (DNA-PKcs, Ab-4), Cell Signaling Technology (phospho-Chk1 S345, no.2341), and Santa Cruz Biotechnology (Chk1, G-4). Cell preparation for staining of 53BP1, γH2AX and incorporated BrdUrd was performed as described (9). For RPA2 and Rad51 staining, cells were preextracted with phosphate-buffered saline containing 0.1% Triton X-100. The fixed cells were incubated with primary antibodies specific for 53BP1, BrdUrd, γH2AX, and Rad51. After incubation with secondary antibodies, cell nuclei were stained with 4′,6-diamidino-2-phenylindole (2 μg/ml). A Carl Zeiss Axiovert 200 fluorescence microscope or LSM510 laser-scanning microscope was used to visualize samples.

Western Blotting—Cell lysis, SDS-PAGE, and gel transfer were performed as described (9). After incubation with secondary antibody, the membranes were visualized using SuperSignal chemiluminescent substrate (Pierce).

Cell Cycle Synchronization and Flow Cytometry—To synchronize cells in the S phase, cells were treated with thymidine at 2.5 mM for 18 h and incubated with a fresh medium for 5 h. To collect G_1 phase cells, cells were treated with nocodazole for 12 h and released with a fresh medium for 5 h. For cell cycle analysis, cells were harvested and stained with propidium iodide after fixing with 70% ethanol. Propidium iodide-stained cells were analyzed using a FACSCalibur (BD Biosciences).

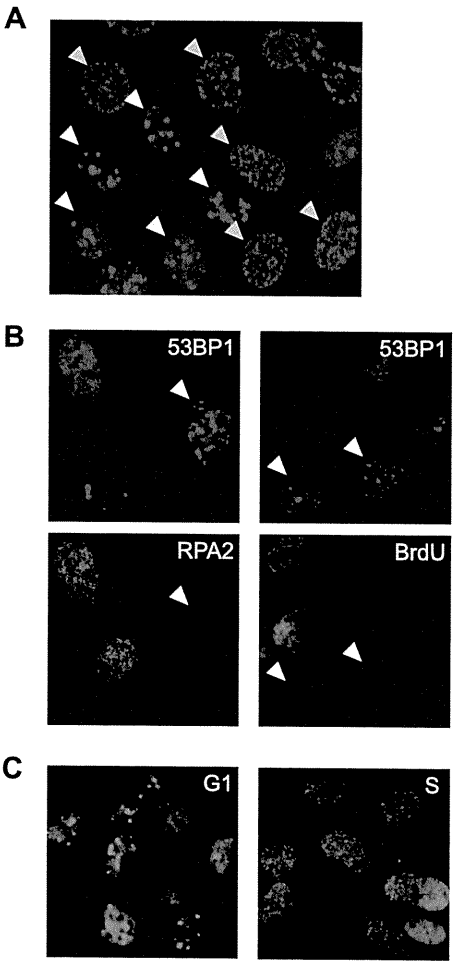

FIGURE 1. **CPT induces two distinct types of 53BP1 foci.** *A*, representative image of 53BP1 foci induced by CPT (2 μM, 1 h) treatment. The HeLa cells denoted by *white arrowheads* represent Type I 53BP1 foci, whereas *yellow arrowheads* denote Type II foci. *B*, Type I 53BP1 foci occurring in non-S phase cells. HeLa cells were treated with CPT (2 μM, 1 h) and stained with anti-53BP1 and RPA2 antibodies (*left*). To observe DNA synthesis, cells were treated with BrdUrd (20 μM, 20 min) and stained with α-53BP1 and α-BrdUrd antibodies (*right*). *C*, CPT-induced 53BP1 foci in G_1 or S phase cells. Cells were synchronized in G_1 phase and S phase by release from nocodazole block and thymidine block, respectively. After treatment with CPT (2 μM, 1 h), cells were stained with anti-53BP1 antibody.

Neutral Comet Assay—Cells were suspended in 0.7% low melting point agarose and spread on glass slides precoated with 1% agarose. Slides were overlaid with coverslips that were removed after the gel solidified. The gel was treated with lysis solution (Trevigen) for 30 min at 4 °C in the dark and electrophoresed at 1 V/cm for 17 min. Comet tails were stained with SYBR Green I (BMA) and analyzed by fluorescent microscope.

RESULTS

CPT Induces Two Types of 53BP1 Foci in Mammalian Cells—53BP1 is an adaptor protein that is recruited to nuclear foci in response to genotoxic stimuli, including ionizing radiation-induced DSBs and CPT-associated DSEs (11, 12). Following the treatment of HeLa cells with CPT, we observed two distinct 53BP1 localization patterns: Type I exhibited large 53BP1 foci that typically numbered fewer than 15/cell; Type II displayed

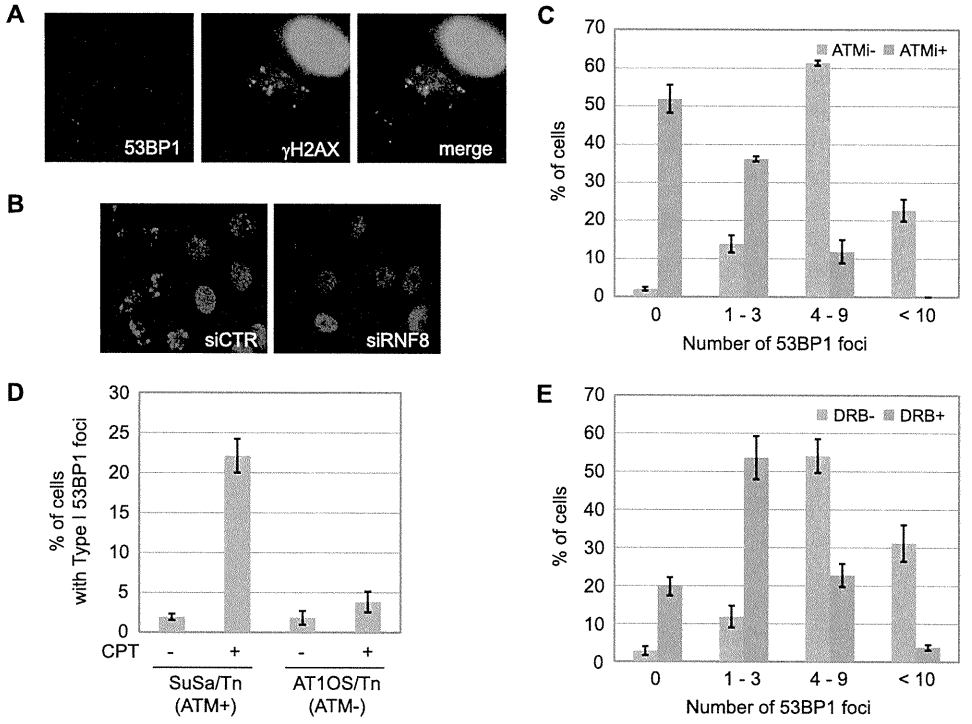

FIGURE 2. **Type I 53BP1 foci are ATM-dependent and occur in response to transcription-mediated DNA damage.** *A*, co-staining 53BP1 with γH2AX. HeLa cells were treated with CPT (2 μM, 1 h) and stained with α-53BP1 and γH2AX antibodies. *B*, formation of 53BP1 foci requiring RNF8. HeLa cells were transfected with nontargeting (*siCTR*) or RNF8-targeting siRNA (*siRNF8*) and stained with anti-53BP1 antibody following CPT (2 μM, 1 h) treatment. *C*, effect of ATM inhibition on Type I 53BP1 foci formation. HeLa cells were treated with solvent only, KU-55933 (10 μM, 1 h) before CPT (2 μM, 1 h) treatment, and stained with anti-53BP1 and anti-RPA2 antibodies. *D*, Type I 53BP1 foci in ATM-deficient cells. Control cells (*SuSa/Tn*) and ATM-deficient cells (*AT1OS/Tn*) were treated with CPT (2 μM, 1 h) and stained with anti-53BP1 and anti-RPA2 antibodies. *E*, effect of transcription inhibition on Type I 53BP1 foci formation. HeLa cells were treated with DRB (100 μM, 2 h) before CPT (2 μM, 1 h) treatment and stained with anti-53BP1 and anti-RPA2 antibodies. The number of 53BP1 foci observed in cells without RPA2 signal was counted. *Error bars* show S.E. calculated from three independent experiments.

many smaller foci (Fig. 1*A*). To characterize Type I and Type II foci further, we co-stained the cells with antibodies specific for the 32-kDa subunit of replication protein A (RPA2) following cellular preextraction with detergent. The presence of detergent-resistant RPA2 foci was used to distinguish S phase cells from G_1 phase cells (13). We found that cells possessing Type I 53BP1 foci were not co-stained for RPA2, whereas cells possessing Type II 53BP1 foci were (Fig. 1*B*). This finding suggested that Type I 53BP1 foci are formed predominantly in non-S phase cells. Consistent with this idea, cells displaying Type I 53BP1 foci did not incorporate BrdUrd, supporting the assertion that they are in either in G_1 or G_2/M phase (Fig. 1*B*). To substantiate this finding further, we used cell cycle synchronization to show that G_1 phase cells treated with CPT displayed Type I 53BP1 foci, whereas Type II 53BP1 foci were predominantly observed in S phase cells following CPT treatment (Fig. 1*C*). These results raised the possibility that Type I, DNA replication-independent, 53BP1 foci are caused by transcription-mediated DNA damage.

Formation of Type I 53BP1 Foci Requires RNF8, ATM, and Active Transcription—To characterize the CPT-induced Type I 53BP1 foci further, we examined co-localization of 53BP1 with a well established marker of DNA damage, phosphorylated-H2AX (γH2AX). We found that Type I foci were co-localized with γH2AX. On the other hand, γH2AX showed an intense, pan-nuclear signal in cells displaying Type II 53BP1 foci (Fig. 2*A*). The E3 ubiquitin ligase RNF8 is required for 53BP1 foci formation in response to DSBs induced by IR (14–16), and we found that RNF8 knockdown also sharply suppressed CPT-induced 53BP1 foci (Fig. 2*B* and supplemental Fig. S1). To test for the dependence of this response on ATM, HeLa cells were treated with the ATM inhibitor KU-55933 coincident with CPT treatment and co-stained with 53BP1 and RPA2. Focusing solely on RPA2-negative, non-S phase cells, we found that the number of Type I 53BP1 foci/cell was suppressed in KU-55933-treated cells as well as ATM-deficient cells (Fig. 2, *C* and *D*). These findings strongly suggested that Type I 53BP1 foci were formed in an ATM-dependent manner.

CPT interferes with RNA transcription, and transcription-associated DNA damage linked to ATM activation has recently been reported (7). Therefore, we tested the transcription dependence of CPT-induced 53BP1 foci by treating cells with DRB, a CDK inhibitor, that suppresses the phosphorylation of polymerase II C-terminal domain required for transcription elongation (17–19). Cells pretreated with DRB showed a drastic reduction in Type I 53BP1 foci (Fig. 2*E*). Taken together, these data demonstrate that, in non-S phase cells, CPT causes transcription-mediated DNA damage leading to the ATM and RNF8-dependent accumulation of 53BP1 foci.

Transcription-dependent ATM Activation in Response to CPT—The above experiments using DRB suggested that CPT-induced ATM activation is dependent on transcription. However, DNA replication-mediated DSEs are thought to account for the majority of CPT-induced DNA damage. To assess the relative contributions of transcription-associated *versus* replication-associated DNA damage to the activation of downstream pathways, HeLa cells were pretreated with inhibitors of DNA replication and transcription prior to the addition of CPT. Treatment with the replication inhibitor HU for 10 min effectively suppressed DNA synthesis (supplemental Fig. S2) and virtually abolished CPT-induced RPA2 phosphorylation (Fig. 3, *left*). Thymidine treatment prior to CPT addition also suppressed RPA2 phosphorylation (Fig. 3, *left*), indicating that RPA2 phosphorylation is highly dependent on DNA replication. In contrast, neither CPT-induced ATM autophosphorylation on Ser^{1981} nor ATM-dependent phosphorylation of Chk2 on Thr^{68} was suppressed by DNA replication inhibition

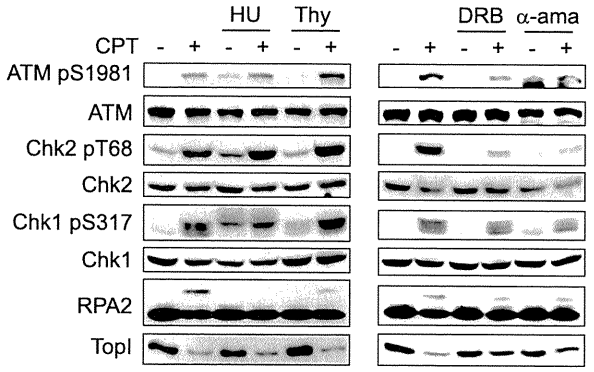

FIGURE 3. **Transcription-dependent ATM activation in response to CPT.** HeLa cells were pretreated with DNA replication inhibitors (HU and thymidine (Thy), 2 mM and 2.5 mM, respectively) or transcription inhibitors (DRB and α-amanitin, 100 μM and 5 μM, respectively) before CPT (2 μM, 1 h) treatment. DNA damage signaling was analyzed by Western blotting using appropriate antibodies.

(Fig. 3, *left*). These results imply that CPT-dependent activation of ATM does not absolutely require DNA replication.

In stark contrast to results using DNA replication inhibitors, the transcriptional inhibitors DRB and α-amanitin apparently suppressed CPT-induced ATM autophosphorylation at Ser^{1981} and Chk2 phosphorylation on Thr^{68} (Fig. 3, *right*). These results are consistent with previous reports demonstrating that CPT-induced ATM activation is dependent on transcription in non-cycling cells (7, 20). Our data further indicate that transcription-coupled events account for the bulk of ATM activation by CPT, even in actively dividing cells. Importantly, the transcription dependence of ATM activation established with CPT was not observed with other DNA-damaging agents, such as IR, the topoisomerase II inhibitor VP-16, and UV light (supplemental Fig. S3). These findings indicate that TopI poisons uniquely induce transcription-coupled DNA damage that signals to ATM.

ATM Is Required for CPT-induced Checkpoint Responses—To examine a possibility that ATM contributes to CPT-induced cell cycle checkpoint regulation, U2OS cells were treated with the ATM inhibitor KU-55933, exposed to CPT, and then monitored in cell cycle distribution by flow cytometry. Whereas U2OS cells treated with dimethyl sulfoxide or the DNA-PK inhibitor NU7026 exhibited prolonged G_1 arrest up to 12 h following CPT treatment, U2OS cells treated with KU-55933 began exiting G_1 phase by 6 h (Fig. 4*A*). This indicates that CPT induces an ATM-dependent G_1/S checkpoint. Consistent with a defect in the G_1/S phase checkpoint, ATM-inhibited U2OS cells rapidly accumulated in the S phase between 6 and 12 h after CPT treatment (Fig. 4*B*). By 24 h after CPT exposure, however, ATM-inhibited cells exited S phase and accumulated in the G_2 phase, which is indicative of a defect in S phase checkpoint maintenance (Fig. 4*B* and supplemental Fig. S4). In contrast, inhibition of DNA-PK did not result in S phase accumulation of U2OS cells at early time points (6–12 h), nor did the inhibitor cause premature S phase checkpoint release (Fig. 4*B*). Together, these results suggest that ATM, but not DNA-PK, is involved in CPT-induced G_1/S and S phase checkpoint activation.

Based on the ATM contribution to S phase checkpoint activation, we further analyzed the effect of ATM on the ATR-Chk1 pathway. Autophosphorylation of ATM Ser^{1981} and DNA-PKcs Ser^{2056} was used to monitor ATM and DNA-PK activation, respectively, whereas Chk1 Ser^{317} phosphorylation was used as a surrogate marker for ATR activation. Treatment with caffeine (2 mM) had no effect on ATM and DNA-PKcs autophosphorylation, but strongly suppressed Chk1 phosphorylation (supplemental Fig. S5), which is consistent with the previous finding that ATR is the primary Chk1-activating kinase in response to TopI poisons (4). ATM inhibition also strongly suppressed Chk1 phosphorylation, indicating that both ATM and ATR are required for full Chk1 activation in response to CPT (supplemental Fig. S5).

To analyze CPT-induced Chk1 phosphorylation further, we performed knockdown of TopBP1, a direct activator of ATR that is required for Chk1 phosphorylation in response to IR, UV, and HU (21). HeLa cells were transfected with siRNA against TopBP1, and the phosphorylation of Chk1, Chk2, and RPA2 was analyzed by Western blotting. CPT-induced Chk1 phosphorylation was suppressed in TopBP1 knockdown cells, whereas Chk2 phosphorylation was not (Fig. 4*C*), implying that CPT-induced Chk1 phosphorylation requires TopBP1 and suggesting that ATM is upstream of TopBP1 in the pathway leading to Chk1 phosphorylation. RPA2 phosphorylation was not suppressed by TopBP1 knockdown (Fig. 4*C*). Given that CPT-induced phosphorylation of RPA2 is reported to be ATR-dependent (22), this finding indicates that ATR can be activated independent of TopBP1 in CPT-treated cells. Finally, we used synchronized HeLa cells to show that CPT-induced TopBP1 and Chk1 phosphorylation are restricted to S phase cells and are dependent on ATM (Fig. 4*D*). From these findings, we propose the existence of an ATM-TopBP1-ATR-Chk1 signaling pathway that is activated by CPT in S phase cells. Because transcription inhibition only slightly affected CPT-induced Chk1 phosphorylation, replication-coupled DSEs, but not transcription-coupled DNA damage, probably trigger this pathway.

Hyperactivation of DNA-PK in ATM-inhibited Cells—The above findings are consistent with a model in which CPT caused the transcription-coupled activation of an ATM-dependent G_1/S checkpoint. Interestingly, we found that CPT-induced activation of DNA-PK was strongly potentiated when ATM was inhibited in HeLa cells (Fig. 5*A*). This result was also observed in ATM-deficient cells (Fig. 5*B*). The enhanced DNA-PKcs autophosphorylation observed in the presence of the ATM inhibitor KU-55933 was suppressed by HU treatment, indicating that DNA-PK hyperactivation by ATM inhibition requires ongoing DNA replication (Fig. 5*A*). This finding is consistent with our earlier report that CPT-induced DNA-PK activation is strongly dependent on DNA replication (23). DRB also partially inhibited CPT-induced DNA-PK autophosphorylation, which is consistent with the notion that transcription-coupled events lie upstream of DNA-PK activation (Fig. 5*A*).

A plausible explanation for the DNA replication and transcription-dependent hyperactivation of DNA-PK in ATM-inhibited cells is that ATM inhibition led to the defect in G_1/S and S phase checkpoints and the carryover of transcription-mediated strand breaks into the S phase, where such lesions were converted to frank DSEs activating DNA-PK. To test this possibility, we used neutral comet assays to assess CPT-induced

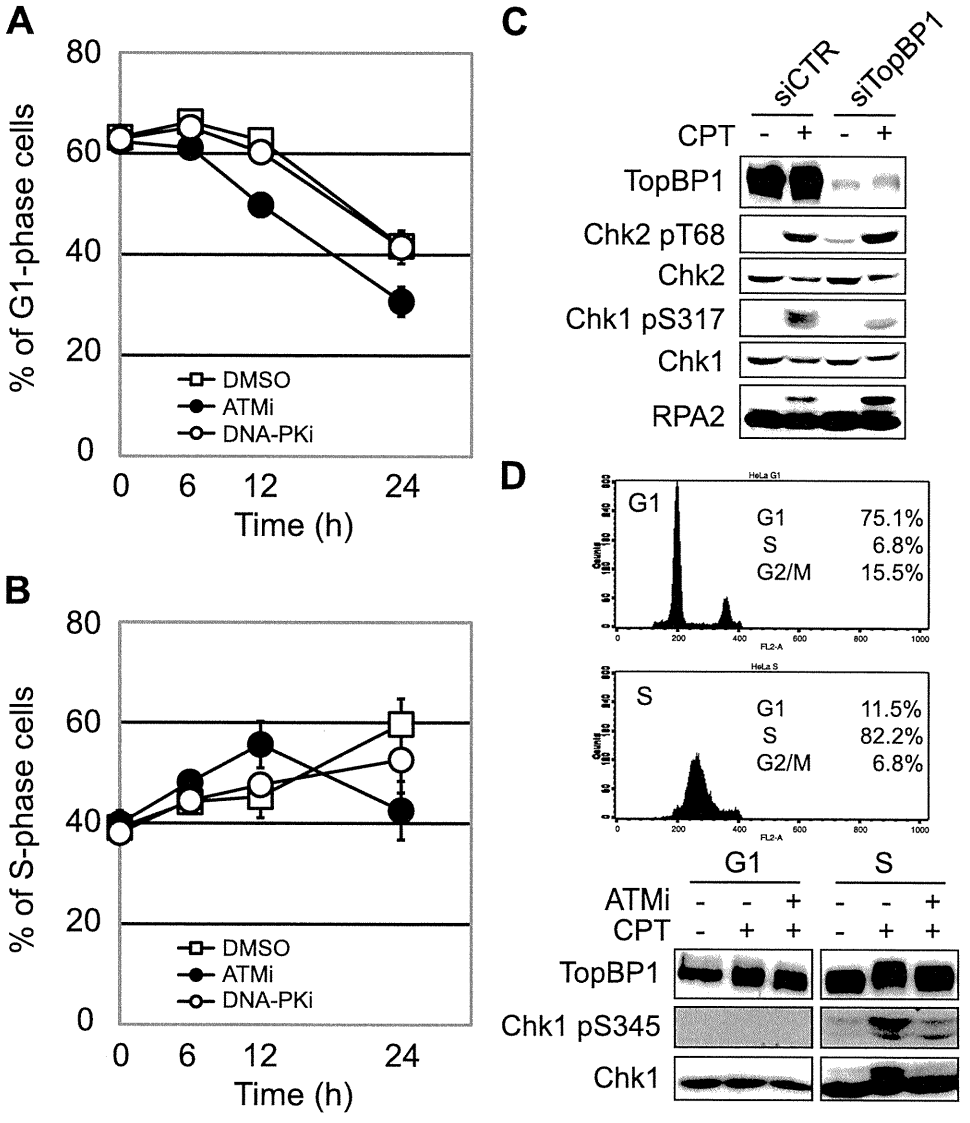

FIGURE 4. **CPT induces ATM-dependent G_1/S and S phase checkpoint arrest.** *A* and *B*, U2OS cells were treated with 1 μM CPT following treatment with ATM (KU-55933; 10 μM, 1 h) or DNA-PK inhibitor (NU7026; 10 μM, 1 h). After incubation for the indicated time, cells were fixed with ethanol for propidium iodide staining. Cell cycle distribution was analyzed by flow cytometry, and the percentage of cells in G_1 phase and S phase was plotted in *A* and *B*, respectively. *Error bars* show S.E. calculated from three independent experiments. *C*, CPT-induced Chk1 phosphorylation is TopBP1-dependent. HeLa cells transfected with control (*siCTR*) or TopBP1 siRNA (*siTopBP1*) were treated with CPT (2 μM, 1 h), and then Chk2, Chk1, and RPA2 phosphorylation were analyzed by Western blotting with the indicated antibodies. *D*, CPT-induced TopBP1 phosphorylation is restricted to S phase. To synchronize cell cycle in the G_1 and S phase, HeLa cells were released from nocodazole block and thymidine block, respectively. Both cell populations were treated with CPT (2 μM, 1 h) with or without ATM inhibitor (KU-55933; 10 μM, 1 h). TopBP1, Chk1, and Chk1 phosphorylation was detected by Western blotting using the indicated antibodies.

DSEs in cells treated with ATM inhibitor or vehicle. As expected, CPT treatment caused an increase in comet tail moment, reflecting the generation of DNA strand breaks (Fig. 5*C*). Cells co-treated with CPT and the ATM inhibitor demonstrated an ~2.5-fold increase in comet tail moment compared with cells treated with CPT alone, supporting the contention that accumulation of DSEs is responsible for DNA-PK hyperactivation in the absence of functional ATM. Finally, as predicted based on the DNA-PK autophosphorylation results, the accumulation of DNA strand breaks in CPT and ATM inhibitor-treated cells was reduced by DRB treatment (Fig. 5*C*). These results are consistent with a model whereby transcription-mediated strand breaks are carried over from G_1 phase to S phase in ATM-inhibited cells, where they are converted into DSEs upon collision with DNA replication forks.

Substantiation of the above model required us to test whether CPT-induced transcription-mediated strand breaks arising in the G_1 phase are in fact responsible for DNA-PK hyperactivation. To test this possibility, U2OS cells were synchronized in the G_1 phase as schematically indicated in Fig. 5*D*. G_1-synchronized cells were incubated with KU-55933 for 1 h prior to CPT exposure. CPT treatment was performed only for 1 h during G_1 phase to avoid the possibility of direct DSE generation in S phase. At 0 h, 1 h, and 5 h after CPT addition, DNA-PKcs autophosphorylation was analyzed by Western blotting. There was no significant difference in S phase percentages between untreated and ATM inhibitor-treated cells in the absence of CPT, indicating that ATM inhibition does not affect S phase entry in this system (Fig. 5*D*). We found that CPT-induced DNA-PKcs autophosphorylation was enhanced in cells treated with the ATM inhibitor in the G_1 phase *versus* cells treated with CPT alone (Fig. 5*D*). Overall, the findings demonstrate that ATM activates a G_1/S checkpoint in response to CPT-mediated transcriptional collapse. Failure of this checkpoint leads to the carryover of transcription-mediated strand breaks into the S phase, resulting in DSE generation and hyperactivation of DNA-PK.

DNA-PK Promotes CPT-induced Cell Death in the Absence of ATM—Given that inhibition of ATM led to DNA-PK hyperactivation in CPT-treated cells, we reasoned that dual inhibition of ATM and DNA-PK would lead to synergistic cell killing by CPT. To address this possibility, the effect of ATM or/and DNA-PK inhibition on CPT-sensitivity was analyzed in HCT116 colon carcinoma cells. In HCT116 cells, we found that ATM inhibition caused moderate CPT hypersensitivity, whereas DNA-PK inhibition actually led to a small, yet reproducible, increase in HCT116 cell survival following CPT treatment (Fig. 6*A*). This result is consistent with previous findings showing that DNA ligase IV- or Ku70-deficient chicken DT40 cells display partial CPT resistance (24, 25). Interestingly, we found that DNA-PK inhibition rescued the CPT-hypersensitive phenotype of ATM-

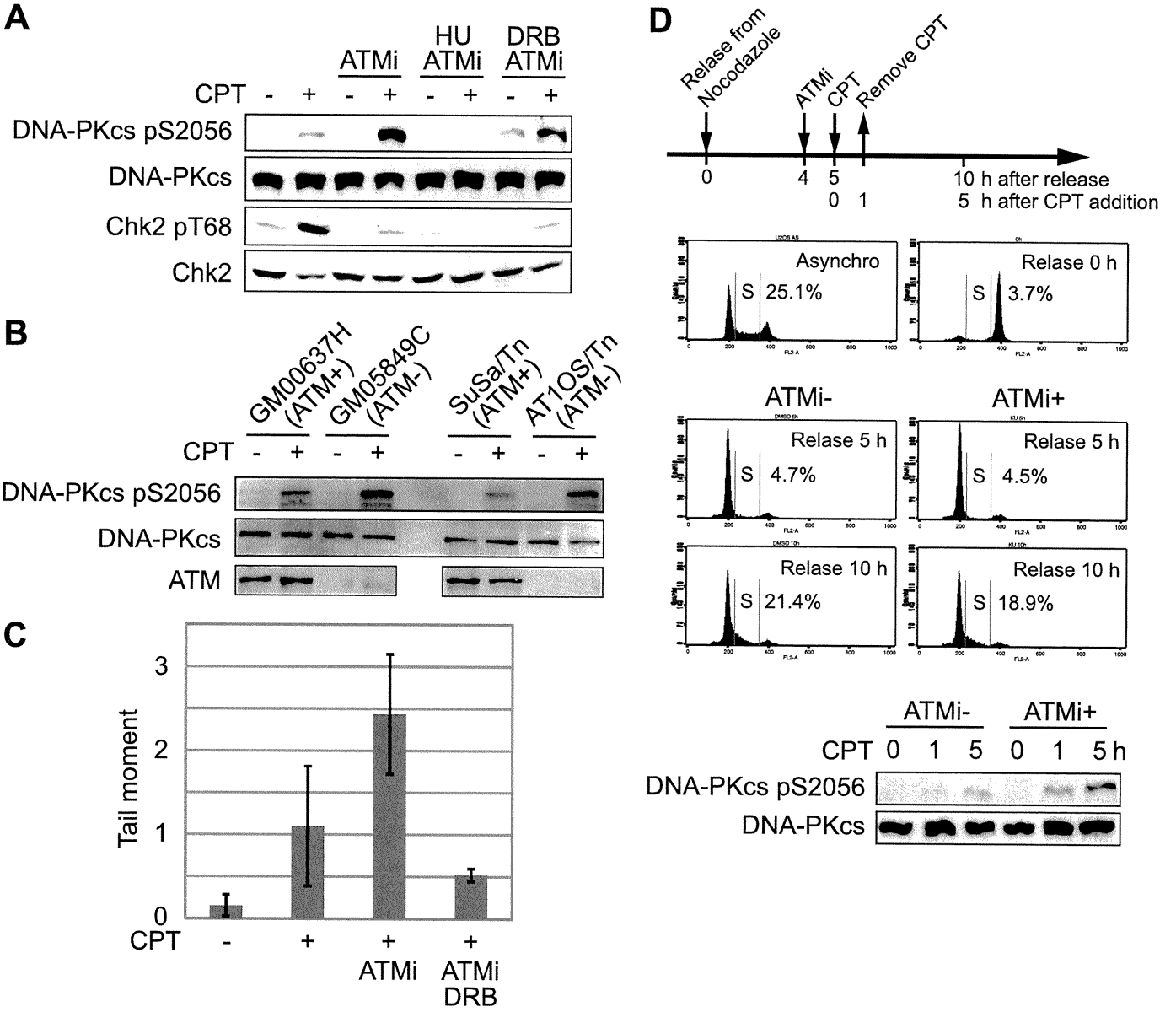

FIGURE 5. **ATM suppresses DNA-PK activation in response to CPT.** *A*, effects of ATM, replication, and transcription inhibitors on CPT-induced DNA-PKcs autophosphorylation. HeLa cells were treated with CPT (2 μM, 1 h) following ATM inhibitor (KU-55933; 10 μM, 1 h) with HU (2 mM, 10 min) or DRB (100 μM, 2 h) treatment, and DNA-PKcs autophosphorylation and Chk2 phosphorylation were analyzed by Western blotting. *B*, DNA-PK activation in ATM-deficient cells. Control cells (GM00637H or SuSa/Tn) and ATM-deficient cells (GM05849C or AT1OS/Tn) were treated with CPT (2 μM, 1 h), and DNA-PKcs autophosphorylation were analyzed by Western blotting. *C*, comet assay for detection of CPT-induced DNA strand breaks. HeLa cells were treated with CPT (0.25 μM) for 1 h following ATM inhibitor (10 μM, 1 h) treatment in the absence or presence of DRB (100 μM, 2 h), and induced-DNA strand breaks were detected by neutral comet assay. The comet tail moments were averaged in triplicate experiments, where the median among 100 cells was calculated in each experiment. *Error bars* represent S.E. calculated from three independent experiments. *D*, inhibition of ATM leads to DNA damage carry over from G_1 to S phase. U2OS cells were synchronized in M phase with nocodazole and released into G_1 and S phase upon incubation with fresh medium. Flow cytometry histograms show cell cycle profiles after release from the nocodazole block in the absence or presence of KU-55933 (10 μM, 1 h). Where indicated, cells were treated with CPT (5 μM, 1 h). The status of DNA-PK activation in the different experimental samples was determined by Western blotting with anti-phospho-DNA-PK antibodies.

inhibited cells (Fig. 6*A*). At a low dose (5 nM) of CPT, HCT116 cells exposed to both DNA-PK and ATM inhibitors showed a 10-fold increase in colony formation *versus* HCT116 cells cultured only in the presence of the ATM inhibitor. This finding suggested that cytotoxicity of CPT is associated with DNA-PK activation.

Given that CPT-induced DSEs are repaired predominantly through HR-dependent pathways in the S phase (2), we reasoned that hypersensitivity of ATM-inhibited cells might be linked to defective HR repair. To test this idea, we measured the formation of Rad51 foci, a surrogate marker for HR, in HeLa cells exposed to CPT in the presence of ATM and DNA-PK inhibitors. CPT treatment for 6 h increased the percentage of cells displaying Rad51 foci from 4% to 11% (Fig. 6*B*). Co-exposure of cells to KU-55933 attenuated CPT-induced Rad51 foci formation, suggesting that ATM contributes to HR repair of these lesions. Surprisingly, the DNA-PK inhibitor treatment also suppressed the percentage of cells with Rad51 foci, and the combination of ATM and DNA-PK inhibition further reduced the percentage of Rad51 foci-positive cells. These findings imply that DNA-PK and ATM cooperatively contribute to the HR pathway in response to CPT and that phe-

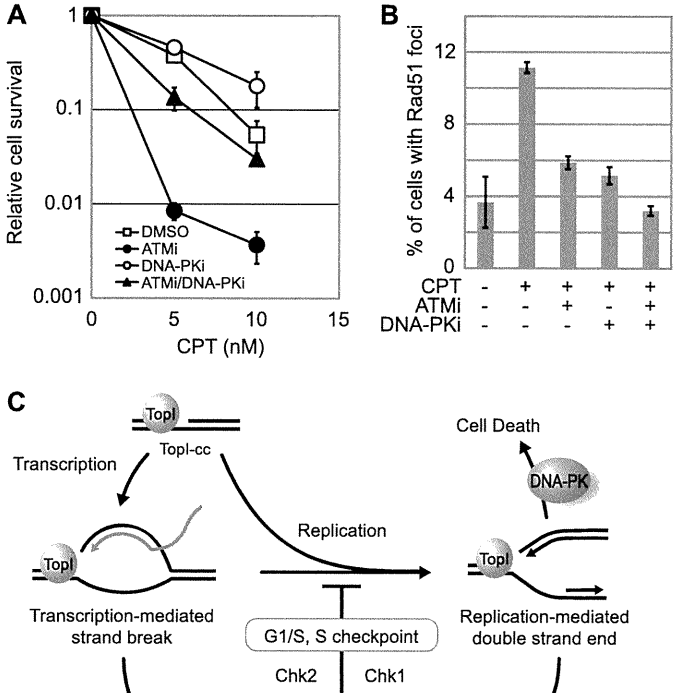

FIGURE 6. **DNA-PK activation promotes cells death in response to CPT.** *A*, clonogenic survival assays of HCT-116 cells treated with CPT in the absence or presence of ATM and/or DNA-PK inhibitors. Cells pretreated with ATM inhibitor (KU-55933; 10 μM, 1 h) and/or DNA-PK inhibitor (NU7026; 10 μM, 1 h) were cultured in the presence of CPT for 2 days at the indicated concentration. *Error bars* show S.E. calculated from three independent experiments. *B*, effects of ATM and/or DNA-PK inhibition on Rad51 foci formation. HeLa cells were treated with CPT (2 μM, 6 h) following pretreatment with ATM (10 μM, 1 h) and/or DNA-PK (10 μM, 1 h) inhibitors, and then cells were stained with anti-Rad51 antibody. The cells with over 10 foci were considered Rad51 foci-positive, and the percentage of Rad51 foci-positive cells is depicted graphically. *Error bars* show S.E. calculated from three independent experiments. *C*, schematic model summarizing the CPT-induced cellular responses. Transcription-mediated strand breaks caused by CPT in G_1 phase are converted to double strand end by DNA replication. ATM is activated against both DNA damages and induces G_1/S and S phase checkpoints to prevent DNA-PK hyperactivation leading to cell death.

notypic rescue of CPT hypersensitivity in cells co-treated with ATM and DNA-PK inhibitors is unlikely due to restoration of HR repair.

DISCUSSION

In this study we have explored the complex mechanisms of signal transduction following exposure of cancer cell lines to a TopI poison, CPT. The most salient findings in the study include: (i) CPT induces transcription-dependent and -independent activation of ATM leading to 53BP1 foci formation and checkpoint activation; (ii) the absence of ATM-dependent G_1/S checkpoint leads to severe DNA damage and DNA-PK hyperactivation in the S phase; (iii) hyperactivation of DNA-PK by CPT in the absence of ATM causes cell death. Taken together, the present findings illuminate important details of the cellular response to a clinically relevant class of chemotherapeutics.

The mechanism of DNA strand breakage induced by CPT and clinically useful derivatives, irinotecan and topotecan, has been the subject of intensive study, and it is well established that TopI-cc are converted to frank DSBs during S phase (1). Transcription-mediated strand breaks are thought to be structurally distinct from DSBs caused by other DNA-damaging agents, such as IR or bleomycin. Because transcription bubbles comprised unwound DNA and nascently synthesized RNA, it is possible that transcription-mediated strand breaks contain a DNA·RNA hybrid end. Consistent with this hypothesis, CPT-induced DNA-PK activation is markedly dependent on DNA replication and was very weak in cells synchronized in G_1 phase. In 1986, Mimori and Hardin (26) reported reduced affinity of the Ku heterodimer for DNA·RNA hybrid probes compared with DNA·DNA double-strand probes. The strong preference of Ku/DNA-PK complexes for double strand DNA *versus* DNA·RNA hybrids plausibly explains why DNA-PK is not activated by CPT in G_1 phase cells. On the other hand, the transcription-dependent activation of ATM, which has been reported here and recently reported by Sordet *et al.* (7), implies that ATM can be activated by DNA·RNA hybrids, although the precise mechanism is not known.

Our results suggested that one end result of transcription-dependent ATM activation is the induction of Chk2 phosphorylation and G_1/S checkpoint arrest. ATM also clearly participates in S phase checkpoint signaling in response to CPT. In S phase cells, ATM promoted TopBP1 phosphorylation and TopBP1-dependent Chk1 activation. The finding implies that ATM and ATR function in a linear pathway, as has been proposed for IR-induced responses (27). Interestingly, CPT-induced RPA2 phosphorylation was not TopBP1-dependent in our hands. Given that ATR is involved in RPA2 phosphorylation (22, 28), this finding implies that TopBP1 is required for only a subset of ATR-dependent phosphorylation events. To summarize these findings, we found that ATM is critical for both G_1 and intra-S phase arrest in response to CPT, which activates two independent ATM activation pathways: a transcription-dependent pathway that is active in the G_1 phase and signals through Chk2, and a DNA replication-dependent pathway that is active in the S phase and signals through TopBP1 and Chk1 (Fig. 6*C*).

In the absence of an ATM-dependent G_1/S checkpoint, transcription-mediated strand breaks caused by CPT are carried over into the S phase, where they are converted into frank DSBs, presumably as a consequence of collisions between stalled transcription complexes and DNA replication forks. As a result, DNA-PK is hyperactivated. In HCT116 cells, the hyperactivation of DNA-PK in the absence of functional ATM leads to a dramatic loss of colony-forming activity. In addition, treatment with only the DNA-PK inhibitor imparted moderate CPT resistance to HCT116 cells, indicating that DNA-PK influences cell survival independent of ATM status. The rescue of CPT sensitivity in ATM-inhibited cells by DNA-PK inhibition cannot be explained by enhanced HR repair because Rad51 foci formation was not promoted by DNA-PK inhibition. Adachi *et al.* (24) have reported similar results showing that DNA ligase IV deletion rescued CPT sensitivity of Rad54-deficient chicken DT40 cells. Although the mechanistic basis for DNA-PK-dependent loss of viability in CPT-treated cells is not clear, we envision two nonexclusive models: first, activation of DNA-PK

could lead to deleterious nonhomologous end joining, which antagonizes survival by promoting deleterious DNA end-joining reactions that preclude HR (24); second, DNA-PK harbors an intrinsic proapoptotic function that is triggered by replication-mediated DSEs. The participation of DNA-PK in apoptosis is complex, with the reports showing prosurvival and proapoptosis functions (29–32). Thus, in the absence of ATM, it is possible that CPT activates a latent, proapoptotic function of DNA-PK. Viewing from a different perspective, our findings raise a question as to how ATM antagonizes DNA-PK-dependent apoptosis in CPT-treated cells. The simplest explanation is that ATM prevents the accumulation of catastrophic S phase damage required to activate DNA-PK. However, it is possible that a more direct antagonism between ATM and DNA-PK exists, at the level of undefined substrate phosphorylation.

In summary, we have shown that ATM responds to CPT-caused transcription collapse and activates cell cycle checkpoints with subsequent prevention of DSE generation and DNA-PK-mediated cell death. These findings indicate that DNA-PK functional status may be an important predictor of CPT treatment efficacy and that pharmacologic abrogation of the G_1/S checkpoint should enhance CPT sensitivity of tumors. These findings provide rationale for further development and preclinical testing of ATM inhibitors and other G_1/S checkpoint modifiers as adjuvants to TopI poison-based therapies.

REFERENCES

1. Pommier, Y. (2006) *Nat. Rev. Cancer* **6,** 789–802
2. Arnaudeau, C., Lundin, C., and Helleday, T. (2001) *J. Mol. Biol.* **307,** 1235–1245
3. Klein, H. L., and Kreuzer, K. N. (2002) *Mol. Cell* **9,** 471–480
4. Cliby, W. A., Lewis, K. A., Lilly, K. K., and Kaufmann, S. H. (2002) *J. Biol. Chem.* **277,** 1599–1606
5. Wang, J. L., Wang, X., Wang, H., Iliakis, G., and Wang, Y. (2002) *Cell Cycle* **1,** 267–272
6. Wu, J., and Liu, L. F. (1997) *Nucleic Acids Res.* **25,** 4181–4186
7. Sordet, O., Redon, C. E., Guirouilh-Barbat, J., Smith, S., Solier, S., Douarre, C., Conti, C., Nakamura, A. J., Das, B. B., Nicolas, E., Kohn, K. W., Bonner, W. M., and Pommier, Y. (2009) *EMBO Rep.* **10,** 887–893
8. Nakamura, H., Fukami, H., Hayashi, Y., Kiyono, T., Nakatsugawa, S., Hamaguchi, M., and Ishizaki, K. (2002) *J. Radiat. Res.* **43,** 167–174
9. Sakasai, R., and Tibbetts, R. (2008) *J. Biol. Chem.* **283,** 13549–13555
10. Dodson, G. E., and Tibbetts, R. S. (2006) *J. Biol. Chem.* **281,** 1692–1697
11. Wang, B., Matsuoka, S., Carpenter, P. B., and Elledge, S. J. (2002) *Science* **298,** 1435–1438
12. Rappold, I., Iwabuchi, K., Date, T., and Chen, J. (2001) *J. Cell Biol.* **153,** 613–620
13. Dimitrova, D. S., and Gilbert, D. M. (2000) *Exp. Cell Res.* **254,** 321–327
14. Mailand, N., Bekker-Jensen, S., Faustrup, H., Melander, F., Bartek, J., Lukas, C., and Lukas, J. (2007) *Cell* **131,** 887–900
15. Kolas, N. K., Chapman, J. R., Nakada, S., Ylanko, J., Chahwan, R., Sweeney, F. D., Panier, S., Mendez, M., Wildenhain, J., Thomson, T. M., Pelletier, L., Jackson, S. P., and Durocher, D. (2007) *Science* **318,** 1637–1640
16. Huen, M. S., Grant, R., Manke, I., Minn, K., Yu, X., Yaffe, M. B., and Chen, J. (2007) *Cell* **131,** 901–914
17. Sehgal, P. B., Derman, E., Molloy, G. R., Tamm, I., and Darnell, J. E. (1976) *Science* **194,** 431–433
18. Peng, J., Zhu, Y., Milton, J. T., and Price, D. H. (1998) *Genes Dev.* **12,** 755–762
19. Dubois, M. F., Bellier, S., Seo, S. J., and Bensaude, O. (1994) *J. Cell. Physiol.* **158,** 417–426
20. Lin, C. P., Ban, Y., Lyu, Y. L., Desai, S. D., and Liu, L. F. (2008) *J. Biol. Chem.* **283,** 21074–21083
21. Liu, S., Bekker-Jensen, S., Mailand, N., Lukas, C., Bartek, J., and Lukas, J. (2006) *Mol. Cell. Biol.* **26,** 6056–6064
22. Sakasai, R., Shinohe, K., Ichijima, Y., Okita, N., Shibata, A., Asahina, K., and Teraoka, H. (2006) *Genes Cells* **11,** 237–246
23. Sakasai, R., Teraoka, H., and Tibbetts, R. S. (2010) *DNA Repair* **9,** 76–82
24. Adachi, N., So, S., and Koyama, H. (2004) *J. Biol. Chem.* **279,** 37343–37348
25. Hochegger, H., Dejsuphong, D., Fukushima, T., Morrison, C., Sonoda, E., Schreiber, V., Zhao, G. Y., Saberi, A., Masutani, M., Adachi, N., Koyama, H., de Murcia, G., and Takeda, S. (2006) *EMBO J.* **25,** 1305–1314
26. Mimori, T., and Hardin, J. A. (1986) *J. Biol. Chem.* **261,** 10375–10379
27. Yoo, H. Y., Kumagai, A., Shevchenko, A., Shevchenko, A., and Dunphy, W. G. (2007) *J. Biol. Chem.* **282,** 17501–17506
28. Anantha, R. W., Vassin, V. M., and Borowiec, J. A. (2007) *J. Biol. Chem.* **282,** 35910–35923
29. Bozulic, L., Surucu, B., Hynx, D., and Hemmings, B. A. (2008) *Mol. Cell* **30,** 203–213
30. Gurley, K. E., Moser, R., Gu, Y., Hasty, P., and Kemp, C. J. (2009) *EMBO Rep.* **10,** 87–93
31. Cobb, L. J., Liu, B., Lee, K. W., and Cohen, P. (2006) *Cancer Res.* **66,** 10878–10884
32. Callén, E., Jankovic, M., Wong, N., Zha, S., Chen, H. T., Difilippantonio, S., Di Virgilio, M., Heidkamp, G., Alt, F. W., Nussenzweig, A., and Nussenzweig, M. (2009) *Mol. Cell* **34,** 285–297

Supplemental figure legends

Figure S1. The effect of RNF8 on CPT-induced Type I foci of 53BP1. HeLa cells were transfected with control siRNA (siCTR) or RNF8 siRNA (siRNF8) and stained with anti-53BP1 antibody following CPT (2 μM, 1 h) treatment. Upper panels are low-power field images and lower is quantitative data of the percentage of cells with Type I 53BP1 foci in duplicate experiments.

Figure S2. DNA synthesis in HU-treated cells. To monitor DNA synthesis, HeLa cells were treated with 2 mM HU for indicated times before BrdU labeling (20 μM, 20 min). Cells were stained with anti-BrdU antibody after denaturation by HCl. Representative images stained by anti-BrdU antibody and DAPI are shown.

Figure S3. Transcription inhibition does not affect ATM activation in response to IR, VP16, or UV. After pretreatment with DMSO or DRB (100 μM, 2 h), HeLa cells were exposed to IR irradiation (2 Gy), VP16 (10 μM), and UV irradiation (10 J/m2) and incubated for 1 h, 1 h, and 2 h, respectively. ATM autophosphorylation and Chk2 phosphorylation were analyzed by Western blotting using specific antibodies.

Figure S4. G2/M arrest of CPT-treated cells. U2OS cells were treated with CPT (1 μM) for indicated time following ATM (10 μM, 1 h) and/or DNA-PK (10 μM, 1 h) inhibitor pretreatment. The percentage of G2/M cells were analyzed by flow cytometery

Figure S5. PIKK activation in response to CPT. HeLa cells were treated with CPT (2 μM, 1 h) following ATM inhibitor (KU55933, 10 μM for 1 h), DNA-PK inhibitor (NU7026, 10 μM for 1 h), caffeine (2 mM for 1 h), or combined treatment. The phosphorylation of indicated proteins were analyzed by Western blotting using appropriate antibodies.

Fig. S1

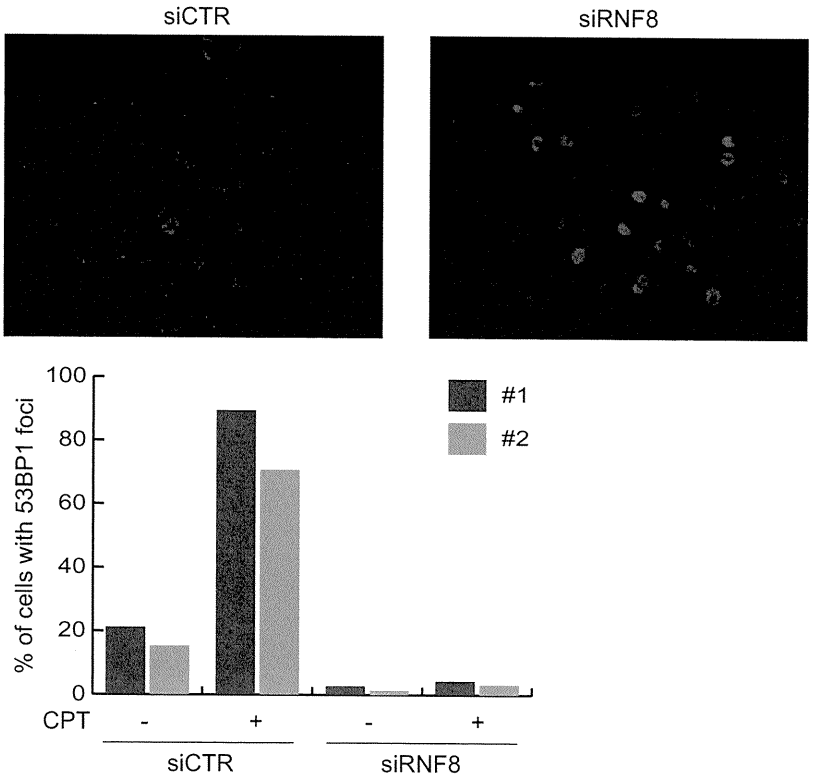

Fig. S2

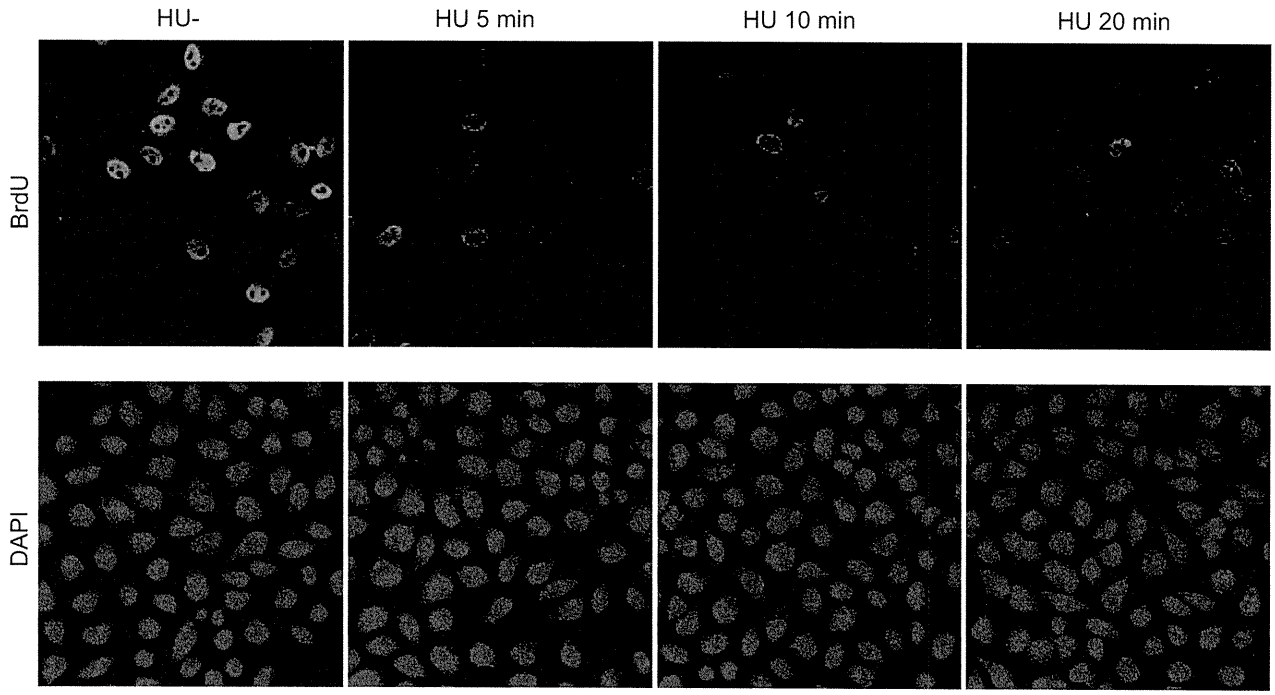

Fig. S3

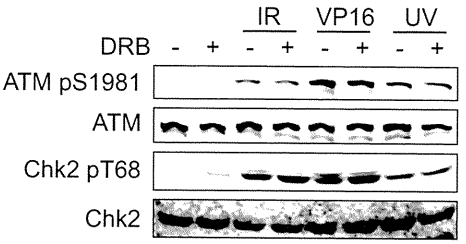

Fig. S4

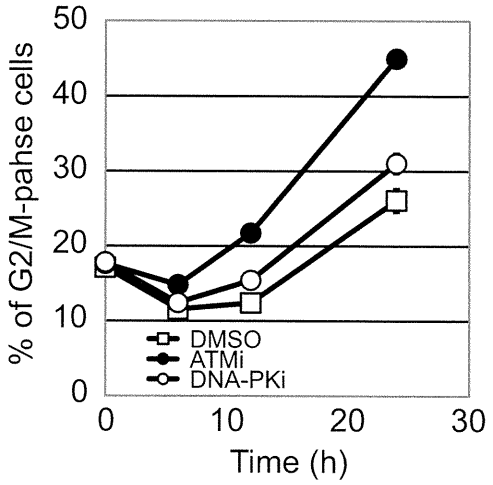

Fig. S5

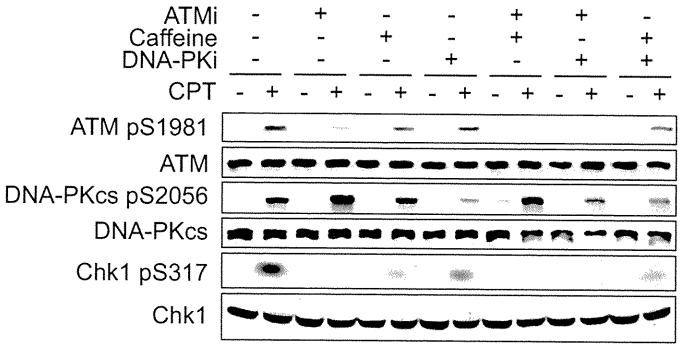

Acta Neuropathol (2010) 119:513–520
DOI 10.1007/s00401-010-0639-4

CASE REPORT

Autopsy study of cerebellar degeneration in siblings with ataxia-telangiectasia-like disorder

Daiju Oba · Masaharu Hayashi · Motoyuki Minamitani · Shinichiro Hamano · Naoki Uchisaka · Akira Kikuchi · Hiroshi Kishimoto · Masatoshi Takagi · Tomohiro Morio · Shuki Mizutani

Received: 21 October 2009 / Revised: 7 January 2010 / Accepted: 9 January 2010 / Published online: 20 January 2010

Abstract Ataxia-telangiectasia-like disorder (ATLD) is caused by mutations of the *MRE11* gene and is characterized by cerebellar ataxia, increased frequency of chromosomal translocations and hypersensitivity to ionizing radiation. ATLD is a rare genetic disease and the associated pathological changes in the brain are unclear. Here, we report the neuropathological findings in the first cases of genetically confirmed ATLD in a pair of Japanese male siblings. Magnetic resonance imaging studies performed during infancy revealed that both subjects had cerebellar atrophy. They died of pulmonary cancer at 9 and 16 years. The siblings had the same compound heterozygous mutations of the *MRE11* gene. Brain autopsy demonstrated mild and severe cerebellar atrophy in the vermis and medial part of the hemispheres, oral to the horizontal fissure, respectively. Nuclear immunoreactivity for MRE11 was absent in neurons of cerebellar cortex, cerebral cortex, basal ganglia and midbrain, whereas being widespread in normal control brains. Immunoreactivity for the DNA oxidative stress marker, 8-hydroxy-2′-deoxyguanosine, was identified in nuclei of granule cells and Bergmann glial cells. The combination of MRE11 deficiency and DNA oxidative injury might have led to selective cerebellar degeneration.

Keywords Ataxia-telangiectasia-like disorder · MRE11 · Cerebellar degeneration · Oxidative stress

D. Oba · M. Minamitani · S. Hamano
Division of Neurology, Saitama Children's Medical Center,
2100, Magome, Iwatsuki-ku, Saitama,
Saitama 339-8551, Japan

M. Hayashi (✉)
Department of Clinical Neuropathology,
Tokyo Metropolitan Institute For Neuroscience,
2-6, Musashi-Dai, Fuchu, Tokyo 183-8526, Japan
e-mail: hayashi-ms@igakuken.or.jp

N. Uchisaka · A. Kikuchi
Division of Hematology/Oncology,
Saitama Children's Medical Center,
2100, Magome, Iwatsuki-ku, Saitama,
Saitama 339-8551, Japan

H. Kishimoto
Division of Pathology, Saitama Children's Medical Center,
2100, Magome, Iwatsuki-ku, Saitama,
Saitama 339-8551, Japan

M. Takagi · T. Morio · S. Mizutani
Department of Pediatrics, Tokyo Medical and Dental University,
1-5-45, Yushima, Bunkyo-ku, Tokyo 113-8519, Japan

Introduction

Ataxia-telangiectasia-like disorder (ATLD) is characterized by cerebellar ataxia, and dysarthria [22]. The clinical features of ATLD are very similar to those of AT caused by mutations in the AT-mutated gene (*ATM*); however, telangiectasia and severe immunodeficiency, which are the cardinal features in AT, are absent in ATLD [1]. ATLD is classified as a chromosomal breakage syndrome because the patients show spontaneously occurring chromosomal aberrations and increased sensitivity to ionizing radiations. ATLD is caused by mutations in the *MRE11* gene [20]. Nijmegen breakage syndrome (NBS), which is caused by mutations in the *NBS1* gene, has also been defined as a chromosomal breakage syndrome, and the main clinical features of NBS are microcephaly, growth retardation, recurrent infections, and predisposition to tumors, but not cerebellar ataxia [22]. ATM, MRE11, and NBS1 are key components of the signaling network involved in cellular response to DNA damage [13]. Neuropathological changes

in AT, characterized by selective cerebellar cortex involvement, are well known [7, 9]. The neuropathological changes in the brains of patients with ATLD have rarely been investigated because of the small number of patients affected by this condition. Here, we report the autopsy findings on the neuropathological changes in Japanese siblings with genetically confirmed ATLD. In addition, we immunohistochemically examined the expression of MRE11 in the human brain and the role of oxidative stress in cerebellar degeneration.

Case report

The clinical and biomolecular findings in these patients have been reported in our previous publication [24]. Here, we briefly outline the genetic characteristics. Family history of the patients was negative for neuromuscular or hematological disorders, and the parents were healthy and non-consanguineous. The patients had an elder brother who did not have any neuromuscular or hematological disorders. The two younger brothers had the same compound heterozygous mutations of the *MRE11* gene (c.727 T>C and g.24994 G>A). The father was a carrier of the c.727 T>C mutation, and the mother and the eldest brother were carriers of the g.24994 G>A mutation. These mutations were novel, and have not been reported in the earlier cases [24]. Western blot analysis revealed severely decreased NBS1 expression, associated with decreased levels of MRE11 and RAD50 in both the subjects. However, *NBS1* gene mutation was not identified.

Subject 1 was born at 37 weeks after an uneventful delivery, with a birth weight of 3,035 g. He showed slight delay in psychomotor development. He started walking independently and uttering words at the age of 1 year and 6 months. His intelligence quotient, measured at the age of 6 years, was 75. During infancy, he gradually developed an unsteady gait and difficulty in coordination of movements of the upper and lower extremities; however, nystagmus was not observed. Brain magnetic resonance imaging (MRI) revealed mild cerebellar atrophy (Fig. 1a, c). An interstitial pulmonary shadow was visible on chest roentgenographs from the age of 3 years. The roentgenograph also revealed atelectasis and an infiltrative shadow in the right lung at the age of 9 years. The lung biopsy demonstrated poorly differentiated adenocarcinoma. He developed right knee pain and bone scintigraphy indicated a metastatic tumor. The combination of cerebellar ataxia and cancer suggested the possibility of AT, but the presence of ATM protein was demonstrated with Western blot analysis

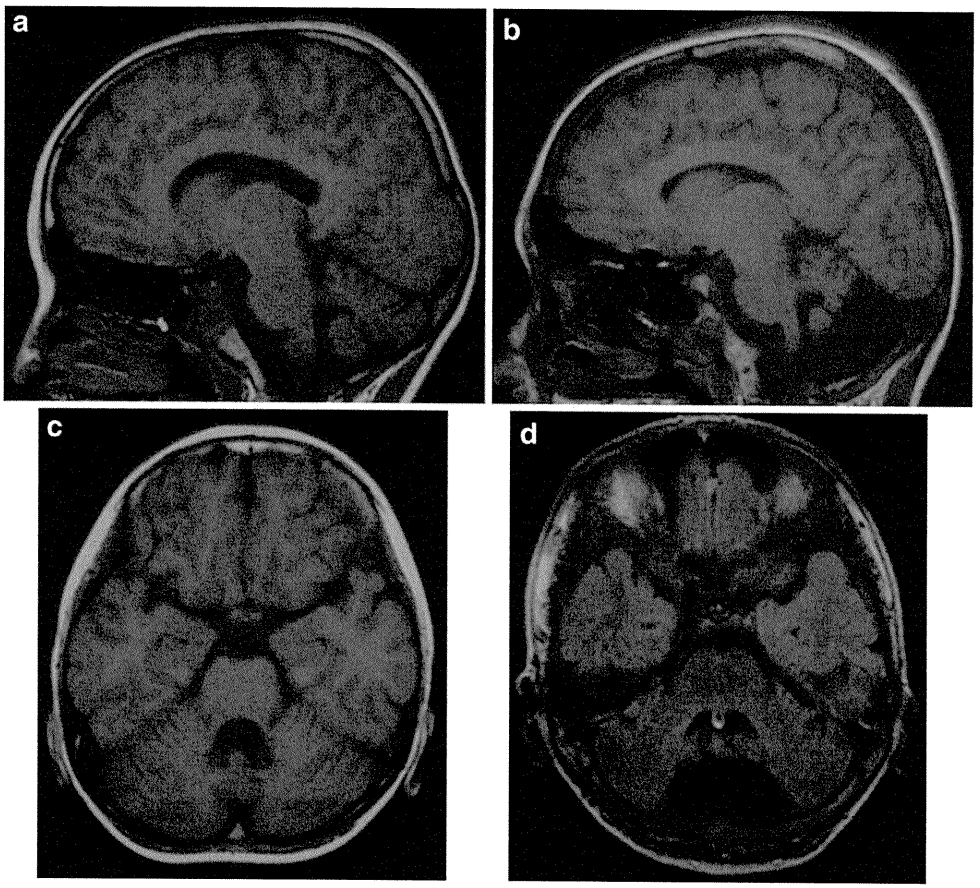

Fig. 1 MRI findings. Subject 1 showed mild (**a**, **c**), while subject 2 showed severe (**b**, **d**) cerebellar atrophy in the vermis and hemisphere. T1-weighted sagittal images (**a**, **b**) and axial image (**c**). **d** An axial image obtained using fluid-attenuated inversion recovery

[24]. Therefore, analysis of the *MRE11* gene was performed. Chemotherapy was ineffective, and the patient died of respiratory failure at the age of 9 years.

Subject 2 was born at 39 weeks after an uneventful delivery, with a birth weight of 2,850 g. He also showed a slight delay in psychomotor development. He started walking independently and uttering words at the age of 1 year and 6 months and 2 years, respectively. He started developing a gait disturbance at the age of 1 year and 11 months. He tended to stumble and could not walk independently at the age of 10 years. Other signs and symptoms of the patient included scanning speech, dysarthria, finger tremor, disturbance of coordinated movements in the extremities, and limitation of ocular movements at the age of 13 years; however, nystagmus was not observed. His intelligence quotient, measured at the age of 14 years, was 43. Brain MRI demonstrated severe cerebellar atrophy (Fig. 1b, d), and ^{121}*N*-isopropyl-p-(123)I iodoamphetamine -single photon-emission computed tomography exhibited hypoperfusion in the cerebral cortex and basal ganglia. At 15 years, he manifested frequent vomiting, disturbed oral uptake, weight loss, and shoulder pain. He also developed increase in serum titers of KL-6 (1,093 IU/ml) and CA125 (967.2 IU/ml). On the basis of the clinical course taken by subject 1, lung biopsy was done, and he was diagnosed with pulmonary adenocarcinoma with bone metastasis. Chemotherapy was ineffective, and he died of respiratory failure at the age of 16 years.

Subject 1 had infiltration of adenocarcinoma in the left lung. Tumor metastasis was identified in the bone marrow; subserosal tissue of the stomach; and lymph nodes in the pulmonary hilus and around the esophagus and stomach. The subject also had congestion of the liver, spleen, and kidneys in addition to ulcer in the middle esophagus. Subject 2 showed infiltration of adenocarcinoma in both lungs. Tumor metastasis was detected in the bones and pulmonary hilar lymph nodes. The subject also had nodular congestion with hemorrhage in the liver and spleen, in addition to edematous swelling in the kidneys.

Materials and methods

Neuropathological examination

The whole brain was fixed with 10% buffered formalin, and brain specimens were embedded in paraffin. Histological examinations were performed on 10-μm thick sections using hematoxylin–eosin (HE), Klüver–Barrera (KB), Bodian, Holzer, and Gallyas–Braak staining methods. For immunohistochemical analyses, 6-μm thick sections were serially cut in selected brain regions, including the frontal cortex, temporal cortex with hippocampus, striatum, thalamus, cerebellum, and midbrain in the ATLD subjects and two controls aged 5 and 16 years. The control subjects had no neurological abnormalities, died from pneumonia and showed no morphological changes in the brain. The sections were de-paraffinized, quenched with 1% hydrogen peroxide, and incubated after microwave or autoclave antigen retrieval, with the following antibodies: mouse monoclonal antibodies to MAP2 (Upstate Cell Signaling Solutions, New York, USA), GFAP (pre-diluted antibody) (Nichirei, Tokyo, Japan), calbindin-D28K, calretinin, parvalbumin (Novocastra Laboratories, Newcastle upon Tyne, UK), 8-hydroxy-2′-deoxyguanosine (8-OHdG), 4-hydroxynonenal (4-HNE) (Japan Institute for the Aging, Shizuoka, Japan), advanced glycation end product (AGE; Trans Genic Inc., Kumamoto, Japan), and rabbit polyclonal antibodies to MRE11 (Calbiochem affiliated to Merck KGaA, Darmstadt, Germany). Antibodies were used at the following concentrations: 1:40 (MRE11), 1:100 (MAP2, calbindin-D28K, calretinin, and parvalbumin), and 1:2,000 (8-OHdG, 4-HNE, and AGE). Antibody binding was visualized by means of the avidin–biotin–immunoperoxidase complex method (Nichirei, Tokyo, Japan) following the manufacturer's protocol. No staining was observed in the sections incubated in the absence of either antibody.

Results

Neuropathological findings

The neuropathological findings in most of the brain areas examined were similar in both subjects. The brain weighed 1,183 and 1,080 g in subjects 1 and 2, respectively. The cerebrum and cerebellum were proportionally small, and the size of the cerebellum was smaller in subject 2 than in subject 1. The gyration of the cerebrum appeared normal (Fig. 2a, b). Coronal brain sections revealed no macroscopic changes in the cerebral cortex, white matter, diencephalon, and ventricular system (Fig. 2c, d). Microscopically, the lamination and interface between the gray and white matters were well preserved in the cerebral cortex. The amygdala and hippocampus did not show any changes. In the globus pallidus, pseudocalcification was seen in subject 1, while perineuronal space dilation was seen in subject 2. Neither neuronal loss nor gliosis was detected in the striatum, thalamus, hypothalamus, and Meynert and subthalamic nuclei in HE, KB, Holzer staining or immunostaining for MAP2 or GFAP. In the cerebellum, subjects 1 and 2 showed moderate to severe atrophy in the vermis orally to the horizontal fissure (central lobule, culmen, declive, and folium) (Fig. 3). Subjects 1 and 2 also revealed mild to moderate atrophy in

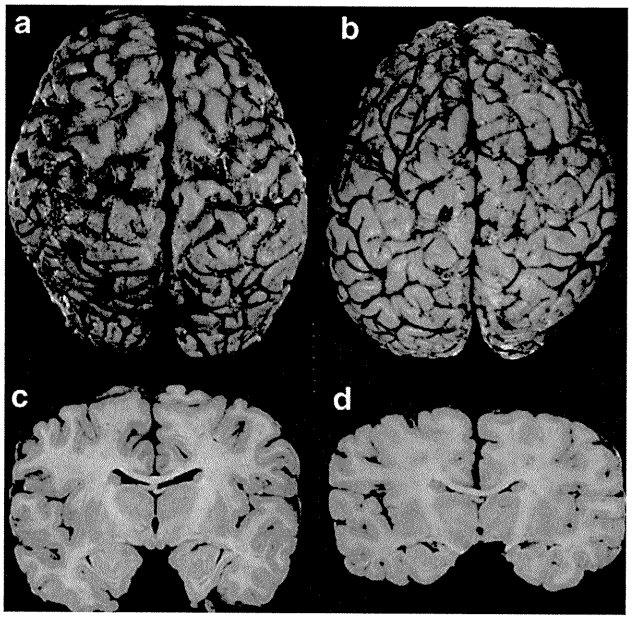

Fig. 2 Macroscopic findings: the surface of the cerebrum appeared normal in subjects 1 (**a**) and 2 (**b**). The coronal brain sections did not reveal any macroscopic changes in the cerebral cortex, white matter, diencephalon, or ventricular system in subjects 1 (**c**) and 2 (**d**)

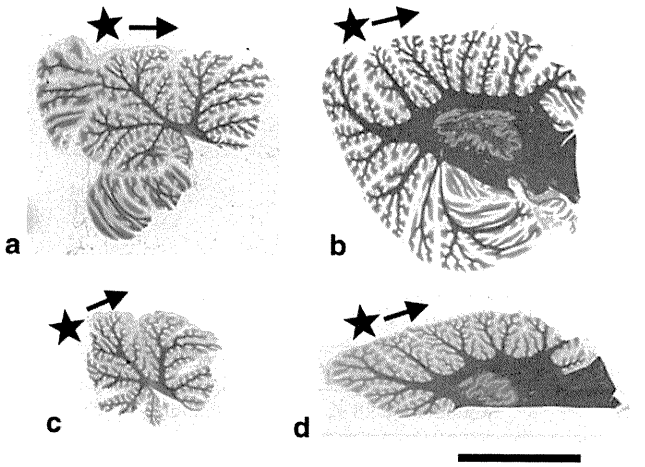

Fig. 3 Sagittal sections of the vermis and cerebellar hemisphere. The vermis (**c**) and the medial part of cerebellar hemisphere (**d**) in subject 2 were relatively smaller than those (**a**, **b**) in subject 1 (Klüver–Barrera staining; *bars* 2 cm). Each *star* with *arrows* denotes the impaired cortex, orally to the horizontal fissure

the medial part of the quadrangular, simple, and superior semilunar lobules. The number of Purkinje cells and granule cells as well as the thickness of the molecular layer were reduced, but Bergmann glial cells were not increased (Fig. 4a, b). Some of the remaining Purkinje cells showed abnormal arborization of dendrites in the molecular layer and axonal swelling in the granule layer (Fig. 4c, d). In subject 2, metastasis of adenocarcinoma was observed in the molecular and granule layers (Fig. 4e, f). Neurons were comparatively spared in the cerebellar cortex of the flocculonodular lobe. The dentate nucleus showed mild fibrillary gliosis, but no neuronal loss. In both the subjects, neurons were preserved in the nuclei of cranial nerves, red nucleus, substantia nigra, locus ceruleus, pontine nucleus, inferior olivary nucleus, and posterior funiculus in the brainstem, in addition to the anterior horn, Clark column, and intermediolateral nucleus in the spinal cord. Sparing of the brainstem and spinal pyramidal tracts, cerebellar peduncles, and medial and lateral lemniscus was also observed.

Immunohistochemistry

In the superior frontal cortex, the number of neurons immunoreactive for MAP2 and calcium-binding proteins (calbindin-D28K, parvalbumin, and calretinin) was counted in six non-overlapping microscopic subfields at 100-fold magnification using a counting box (1 mm^2), and the mean ± 1SD in density of immunoreactive neurons immunoreactive for each marker was obtained (Table 1). The difference in the averaged number between subjects and controls was statistically evaluated by *t* test, and $P < 0.05$ was judged as significant. There was no significant difference between ATLD subjects and controls in the density of cortical neurons immunoreactive for either MAP2 or the calcium-binding proteins. Nuclear immunoreactivity for MRE11 was found in the neurons in the cerebral cortex, hippocampus, striatum, globus pallidus, hypothalamus, Meynert nucleus, Purkinje cells, midbrain tegmentum, and substantia nigra in both the controls aged 5 and 16 years (Fig. 5a, c). In the Purkinje cells, MRE11 immunoreactivity tended to be more predominant in the nucleoplasm than in the nucleolus. In contrast, ATLD subjects 1 and 2 lacked such MRE11 immunoreactivity in the neurons in the cerebral cortex, basal ganglia, hypothalamus, midbrain, and cerebellar cortex (Fig. 5b, d). Immunoreactivity for 8-OHdG, 4-HNE, or AGE was negative in controls. In the ATLD subjects, however, nuclear immunoreactivity for 8-OHdG was observed in granule cells and, to a lesser extent, in Bergmann glia (Fig. 6a, b), which were adjacent to the remaining Purkinje cells. Nevertheless, this 8-OHdG immunoreactivity was not found in the oral vermis; this demonstrated severe Purkinje cell loss. The foci of pseudocalcification in the globus pallidus of subject 1 were immunoreactive for 4-HNE and AGE (data not shown).

Discussion

In 1999, Stewart et al. [20] identified *MRE11* mutations in four ATLD patients. To date, 16 patients from 6 families

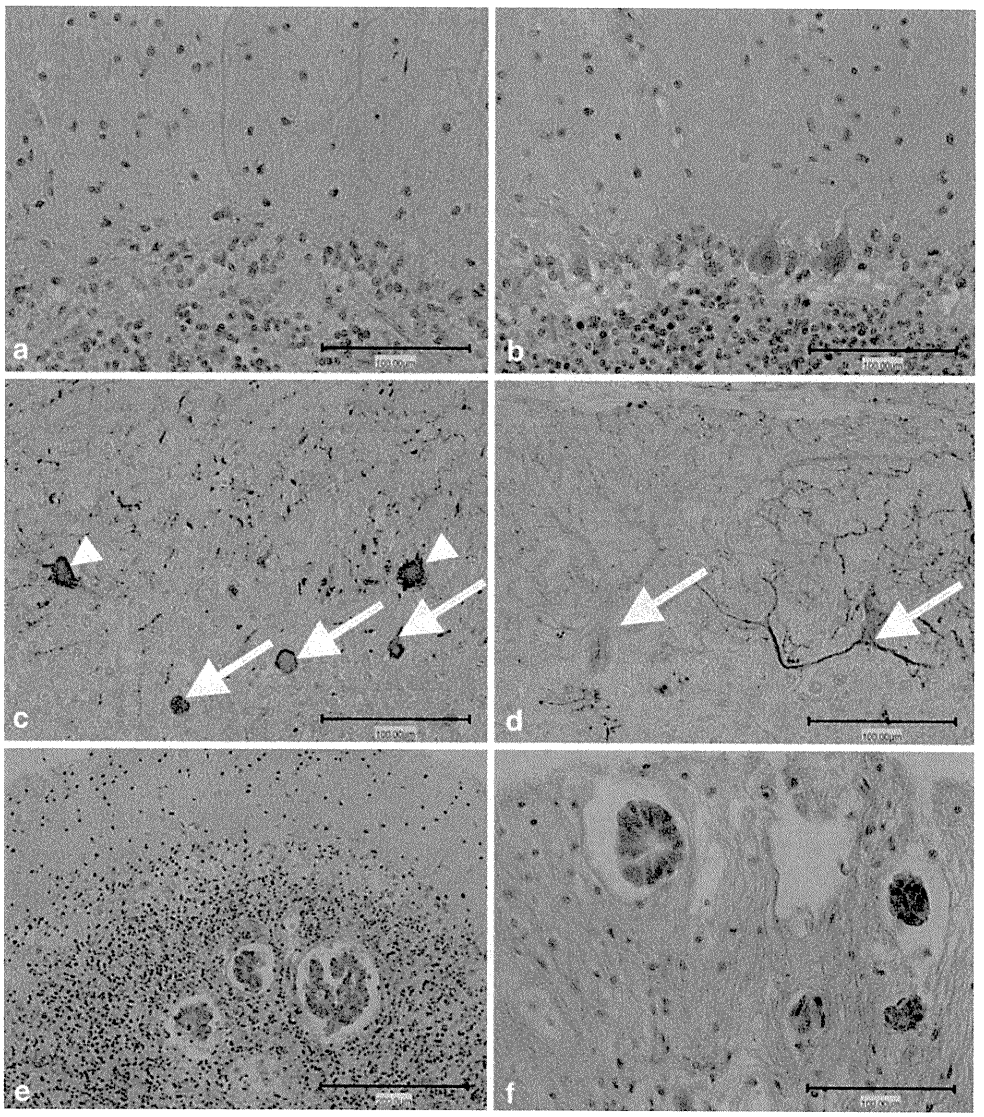

Fig. 4 Histological changes in the cerebellar cortex. In subject 2, the rostral vermis showed loss of Purkinje cells (**a**), whereas the caudal vermis demonstrated preservation of Purkinje cells (**b**) (hematoxylin–eosin stain; *bar* 100 μm). Some of the remaining Purkinje cells showed axonal swellings in the granule layer (**c** *open arrows*; *arrowheads* designate Purkinje cells) and abnormal arborization in the molecular layer (**d** *open arrows*) in subject 1 (**c**, **d**, calbindin-D28K immunostaining; *bars* 100 μm). Tumor metastasis was observed in the granule layer (**e** *bar* 200 μm) and the molecular layer (**f** *bar* 100 μm) in subject 2 (hematoxylin–eosin staining)

Table 1 Quantitative analysis of neurons in the frontal cortex

	Neurons immunoreactive for each marker			
	MAP2	Calbindin-D28 K	Parvalbumin	Calretinin
Mean ± SD per 1 mm^2				
Control 1 (5 years/male)	127.3 ± 5.6	25.3 ± 4.1	25.3 ± 2.7	46.1 ± 8.3
Control 2 (16 years/male)	115.1 ± 11.1	29.8 ± 3.8	31.3 ± 3.6	53.2 ± 6.7
Subject 1 (9 years/male)	120.8 ± 10.5	28.8 ± 5.9	29.2 ± 3.2	52.3 ± 6
Subject 2 (16 years/male)	124 ± 13.5	34.2 ± 8.2	33.7 ± 7.9	43.5 ± 9.2
P value				
Control 1 versus subject 1	0.061	0.306	0.05	0.25
Control 2 versus subject 2	0.386	0.23	0.601	0.081

have been reported as having ATLD, and the present cases are the first ones involving Japanese siblings [24]. The MRE11/RAD50/NBS1 complex (MRN complex) is believed to act as a sensor of DNA damage [13]. Upon exposure to ionizing radiation, the MRN complex becomes rapidly associated with DNA double-strand breaks and remains at these sites until the damage is repaired [27]. Chromosomal breakage syndromes, such as AT and NBS are well-known disorders associated with a predisposition to malignancy. Patients with AT and NBS are susceptible to leukemia and lymphoma [7, 9], and brain tumor, such as medulloblastoma have been linked to NBS [9]. On the other hand, a

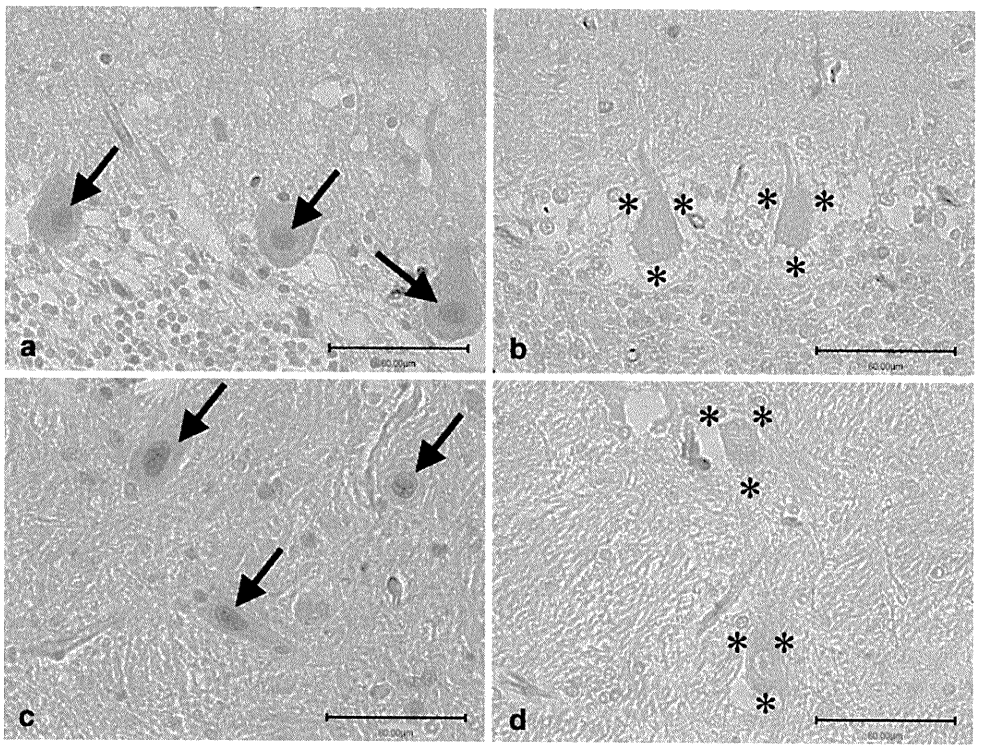

Fig. 5 MRE11 immunostaining. Nuclear immunoreactivity for MRE11 was identified in Purkinje cells in the control aged 16 years (**a** *arrows*) and in neurons of the globus pallidus in the control aged 5 years (**c** *arrows*). Subject 1 lacked neuronal immunoreactivity (*asterisks*) in the same brain regions (**b**, **d**). *Bars* 60 μm

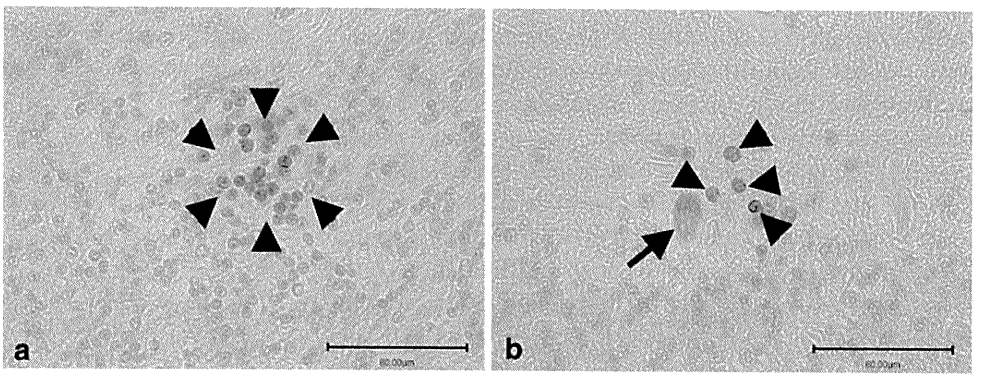

Fig. 6 8-Hydroxy-2′-deoxyguanosine (8-OHdG) immunostaining. Nuclear immunoreactivity for 8-OHdG was detected in granule cells (**a** *arrowheads*) and Bergmann glial cells in subject 1 (**b** *arrowheads*), adjacent to the remaining Purkinje cells (*arrow*). *Bars* 60 μm

predisposition to cancer is not known in ATLD so far [22, 24]. *MRE11* mutations in subjects 1 and 2 may have crucial influence on the functions of MRE11 and presumably have caused the development of lung adenocarcinoma, because they are within the nuclease domain and close to the DNA-binding domain, respectively [24]. Because ATLD and NBS are caused by the loss of function of the MRN complex, and AT is also related to the MRN complex, these three disorders are speculated to have clinical similarities. Nevertheless, AT and ATLD are associated with cerebellar degeneration, whereas NBS patients show microcephaly and preservation of the cerebellum [15, 25]. Other than the reduced brain weight, 4-year-old and 18-year-old NBS patients demonstrated old ischemic necrosis and preserved size and appearance of the cerebellum [25]. Another 31-year-old NBS case showed abnormal location of Purkinje cells and gliosis in the granule layers in the vermis [15]. The recent analysis in mice with hypomorphic mutations of *Mre11* or *Nbs1* demonstrated that DNA damage signaling after genotoxic stress in the nervous system was different between ATLD and NBS and likely explained the respective neuropathology [17]. The neuropathological changes in AT consists of severe atrophy of the cerebellar cortex, predominantly in the vermis, and abnormal dendritic arborization and axonal swelling in the remaining Purkinje cells [7, 9]. In addition, fibrillary gliosis throughout the cerebellar white matter and neuronal loss is observed in the dentate nucleus and inferior olivary nucleus, respectively. Although the changes in the cerebellar white matter, dentate nucleus, and inferior olivary nucleus were limited and subtle, predominant cerebellar cortex atrophy in the vermis was observed in our ATLD subjects. The anterior predominance of vermis atrophy and comparative sparing of the